Metals and Materials International (2021) 27:3079–3084
https://doi.org/10.1007/s12540-020-00610-2

# Corrosion and Oxidation Resistance Behaviors of Ta-Containing Low Alloying Zirconium

Il-Hyun Kim[1,2] · Yang-Il Jung[1,3] · Byoung-Kwon Choi[1] · Hyun-Gil Kim[1] · Jae-Il Jang[2]

Received: 20 November 2019 / Accepted: 3 January 2020 / Published online: 30 January 2020


**Abstract**
Zirconium alloys are widely used to fabricate nuclear fuel claddings, and thus is desirable to improve the resistance of such alloys to corrosion and structural instability. In this study, Ta was used as an alloying element to improve the corrosion and oxidation resistance of zirconium alloys. The model alloy (TaZL) contained 0.03 wt% Ta and other elements with a proportion of less than 1 wt% in total (0.1 wt% Nb, 0.4 wt% Fe, 0.2 wt% Cr) in a zirconium base. The corrosion test involving pressurized water at 360 °C and oxidation test involving steam at 1200 °C indicated that TaZL exhibited the lowest weight gains among those of compared conventional and advanced Zr alloys. The corrosion and oxidation resistances of TaZL were respectively improved by 4 and 1.5 times compared to the corresponding values of Zircaloy-4. The microstructures of the oxide formed on TaZL were columnar along the oxide growth direction and did not change from columnar to equiaxed, which resulted in the high resistance of the alloy to corrosion and oxidation.

**Keywords** Zirconium alloy · Alloy development · Ta · Manufacturing · Microstructure

## 1 Introduction

Improving the corrosion resistance is one of the key concerns in the development of metallic materials. Zirconium exhibits excellent corrosion resistance to high-temperature water, saltwater, and several chemicals. Owing to this high corrosion resistance and its excellent nuclear performance, Zr is widely used in nuclear power plant. Consequently, over the past half century, Zr-based alloys have been evolved to possess a considerably higher resistance to corrosion and oxidation. Zr-based alloys are low alloying materials with the typical alloying elements being Nb, Sn, Fe, and Cr. The elements are added to Zr in a proportion of less than 2.5 wt% in total. The effect of these alloying elements (Nb [1–3], Sn [4, 5], Fe [6, 7], and Cr [7]) on the corrosion behavior of Zr has been investigated thoroughly. In addition, the effect of other minor elements such as Cu [8], Mo [9], V [9], Sb [10], and Ge [11] has been evaluated. These efforts have resulted in the development of commercial alloys, for example, ZIRLO (Zr–1.0Nb–1.0Sn–0.1Fe), M5 (Zr–1.0Nb–0.14O), HANA-4 (Zr–1.5Nb–0.4Sn–0.2Fe–0.1Cr) and HANA-6 (Zr–1.1Nb–0.05Cu).

In this study, Ta was investigated as an alloying element. To the best of our knowledge, Zr alloys for nuclear application have never been alloyed by Ta. Ta is a stable metallic material, which exhibits the formation of $Ta_2O_5$ on its surface [12, 13]. However, the addition of Ta in Zr-based alloys has been avoided because of the high neutron cross-section of the Ta atom. Thus, in this work, the model alloys were fabricated by minimizing the amount of Ta addition. The corrosion and high-temperature steam oxidation behaviors of the fabricated alloy samples were examined.

## 2 Experimental Procedures

The compositions of the alloy considered in this work were Zr–0.1Nb–0.4Fe–0.2Cr–0.03Ta (wt%), and the alloy was named TaZL (Ta-containing zirconium low-alloy). The starting materials with the designated compositions were

✉ Yang-Il Jung
yijung@kaeri.re.kr; yijung@ucla.edu

[1] ATF Technology Development Division, Korea Atomic Energy Research Institute, Daejeon 34057, Republic of Korea

[2] Division of Materials Science and Engineering, Hanyang University, Seoul 04765, Republic of Korea

[3] Mechanical and Aerospace Engineering Department, University of California, Los Angeles, CA 90095, USA

melted in vacuum, and ingots, each with a weight of 200 g, were obtained. The ingots were beta-annealed at 1020 °C for 30 min, and later quenched. To realize hot-rolling, preheating was conducted at 700 °C for 15 min, and the rolling was performed with a reduction rate of 70%. The final heat-treatment was performed at 570 °C for 3 h to obtain the fully recrystallized microstructure. Figure 1 shows the hot-rolled ingot and the microstructure after the final heat-treatment. In the samples, cracking or hardening was not observed during rolling, and full recrystallization was achieved after the heat-treatment.

To conduct the corrosion test, samples with dimensions of 20 mm × 10 mm were cut and ground up to 1200 grit emery paper, and pickled in a 5HF–45$HNO_3$–50$H_2O$ (vol%) solution. The final thickness of the samples after pickling was 1.5 mm. The corrosion test was performed by using a pressurized water loop at 360 °C and 18.5 MPa. The flow rate of the loop was 3–4 L/h. The weight gains of the corroded samples were measured periodically.

To conduct the high-temperature steam oxidation test, samples with dimensions of 10 mm × 10 mm were cut and ground up to 1200 grit emery paper. Under Ar purging, the samples were heated at a rate of 50 °C/min to 1200 °C and maintained at this temperature for 2000s with exposure to a steam supply; the flow rate of the steam supply was 0.5 mL/min. The weight change was measured in situ using a thermogravimetric analyzer (Shimadzu TGA-51H, Japan) with an accuracy of 0.001 mg. To enable comparison, Zircaloy-4 (Zr–1.3Sn–0.2Fe–0.1Cr) samples were tested together with the considered alloy samples.

The surface morphology of the oxides was investigated using a field-emission scanning electron microscope (SEM) (Scios 2, Thermo Fisher, USA). The microstructural characterization of the oxide layer formed during the test was performed using a field-emission high-resolution transmission electron microscope (TEM) (JEM-2100F, JEOL, Japan) at 200 kV. The phases were determined by confirming the atomic ratio as well as the lattice structure. The compositions of the oxide layer were also analyzed using an X-ray diffraction (XRD) spectroscope (XRD SmartLab, Rigaku, Japan).

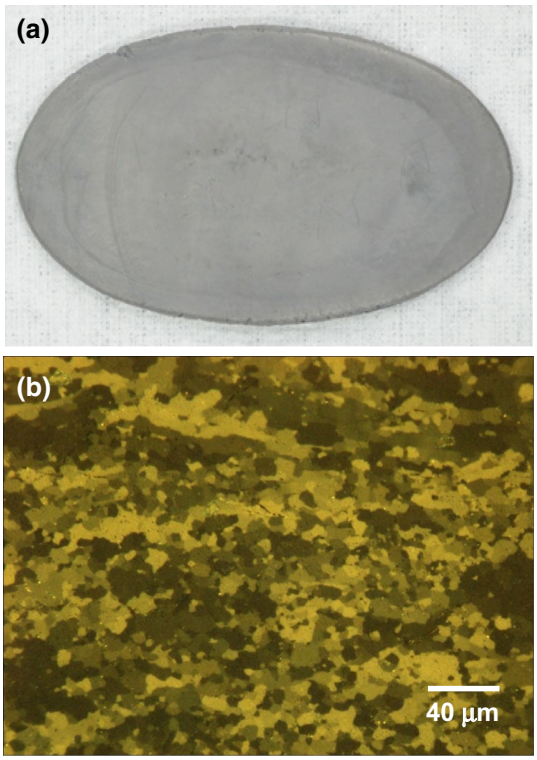


**Fig. 1** **a** Appearance of a model alloy ingot after hot-rolling under a reduction rate of 60%, and **b** its microstructures after final annealing at 570 °C for 3 h

## 3 Results and Discussion

Because a stable and non-dissolving oxide layer is formed on Zr surface during corrosion, the amount of corrosion in Zr alloys can be directly measured by considering the weight gain of the samples. Figure 2 shows the weight gains of samples during the corrosion test. To enable a comparison with other Zr-based alloys, the weight gains of the tested Zircaloy-4 as well as data (HANA-4 and HANA-6) obtained from previous works [14] were plotted together. TaZL demonstrated the lowest weight gain among the compared alloys; the weight gain of TaZL was 54.2 mg/dm$^2$ in 840 days, which was ~75% lower than the weight gain of Zircaloy-4 and ~50% that of HANA-4. The thinner oxide layer can help achieve a high thermal conductivity and mechanical integrity when a Zr alloy is used as a fuel cladding material. The weight gains of TaZL and HANA-6 were similar during the

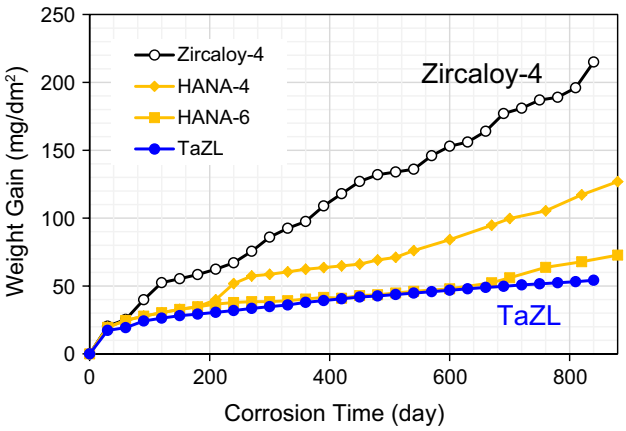


**Fig. 2** Weight gains of various Zr-based alloys during corrosion in 360 °C pressurized water (included comparable data for HANA alloys [14])

initial corrosion stage; however, a kinetic transition (increase in corrosion rate) was observed at 540 days in HANA-6, which resulted in the weight grain of HANA-6 being ~ 20% larger than that of TaZL at the end of the corrosion test.

Figure 3 shows the cross-sectional microstructures of the corroded samples. The oxide layer formed on surface of Zr alloys was clearly distinguished from the substrate. It is observed that the undulant interfaces and rough cross-sectional surfaces of the oxide layer. However, the oxide is known to be stable neither delaminates nor dissolves in pressurized water conditions. Thus, the thickness of oxide indicates the resistance to corrosion of an alloy in concern. The oxide formed on Zircaloy-4 was about three times thicker than that on TaZL. This value underestimates the difference in weight gains (Fig. 2), however, the improvement in corrosion resistance is apparent.

The detailed microstructures of the oxide layers were compared, as shown in Fig. 4. Most of the grains were elongated along the through-thickness direction in both the samples. The columnar structure implies the steady growth of the oxide. The columnar grains are typical microstructures of $ZrO_2$ formed on an oxidized Zr surface [11, 14, 15]. The morphology of the grains can vary from columnar to equiaxed with the thickening of the oxide as the stress accumulated during an oxide growth must be dissipated [14–17]. Equiaxed grains were observed in the oxide formed on Zircaloy-4, as shown in Fig. 4b. The equiaxed structure is often connected to a stable form of oxide; however, it appears as a result of stress built-up in the growing oxide layer. The lateral cracks shown in Fig. 4a also indicate the microstructural transition [14–17]. In contrast, the grains were columnar in the TaZL samples (Fig. 4c–d). The thicker columnar layer in the TaZL samples indicated that the oxide grew thicker without a transitional oxidation when compared to that of Zircaloy-4. Because the transition of the oxide growth makes the oxide more susceptible to the diffusion of the oxygen ions [14, 15], a thicker columnar microstructure is desirable to achieve better oxidation/corrosion resistance. Thus, TaZL exhibits a higher resistance to oxidation than that of Zircaloy-4.

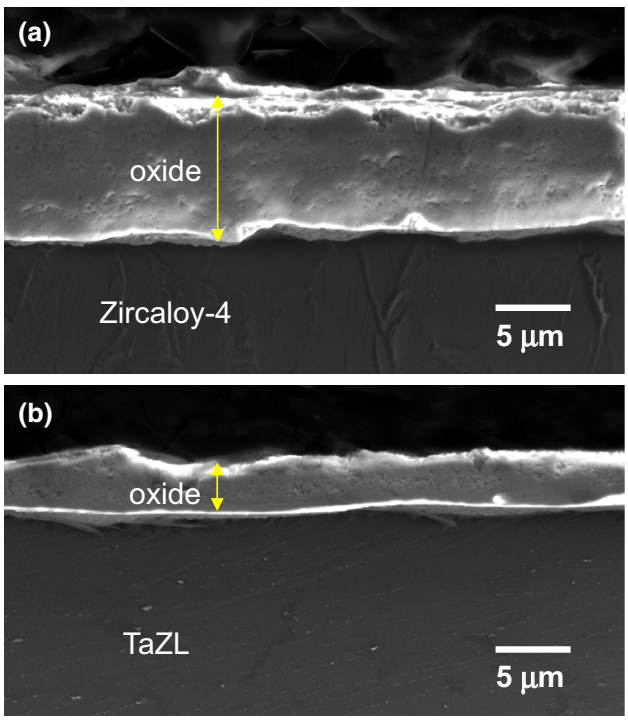


**Fig. 3** Cross-sectional microstructures of samples after a corrosion test, showing the oxide layers formed on the surface of, **a** Zircaloy-4 and **b** TaZL

Figure 5 shows the weight gains of the samples during high-temperature oxidation at 1200 °C in a flowing steam environment. Both TaZL and Zircaloy-4 alloys exhibited parabolic increase in the weight gains without any kinetic transition or breakaway oxidation. As a comparison, weight gains of HANA-4 and HANA-6 were plotted together [18, 19]. The weight gains of HANA alloys lied in between of Zircaloy-4 and TaZL. HANA-4 and HANA-6 revealed lower weight gains than Zircaloy-4 by about 14% and 21%. The weight gain of TaZL was 35% lower than that of the Zircaloy-4. TaZL showed improved resistance to high-temperature oxidation by about 24% and 16% than HANA-4 and HANA-6, respectively.

Figure 6 shows the cross-sectional microstructures of the samples. An examination of the appearance of the samples (add-on images on Fig. 6) indicated the presence of a uniform black oxide all over the TaZL specimens. In contrast, a white oxide was formed on the edges of the specimens of Zircaloy-4. The microstructures demonstrate an accelerated oxidation at the edges of the specimens of Zircaloy-4. In addition, the thickness of the oxide was larger for Zircaloy-4 samples (68 μm) than that for TaZL samples (54 μm).

The chemical compositions of the oxide layer were analyzed using XRD technique. According to the XRD results shown in Fig. 7, the oxides were identified as $ZrO_2$ in both the samples. A shift in the peak positions or additional peaks were not observed in the TaZL samples. In addition, similar microstructures were observed in TEM for the oxidized samples. Although the detailed mechanism of Ta on increasing the oxidation resistance should be defined further, the addition of Ta would be an effective way to develop an enhanced Zr alloy.

Nevertheless, the addition of Ta in Zr-based alloys should be restrained. Ta is harmful to be used in the fabrication of nuclear core materials because of its high thermal neutron capture cross-section (σ). The value of σ for Ta is 21 barns, whereas Zr has a σ value of 0.18 barns. The summation of σ for each element with respect to its atomic ratio in an alloy can help compare the practical applicability of the alloy.

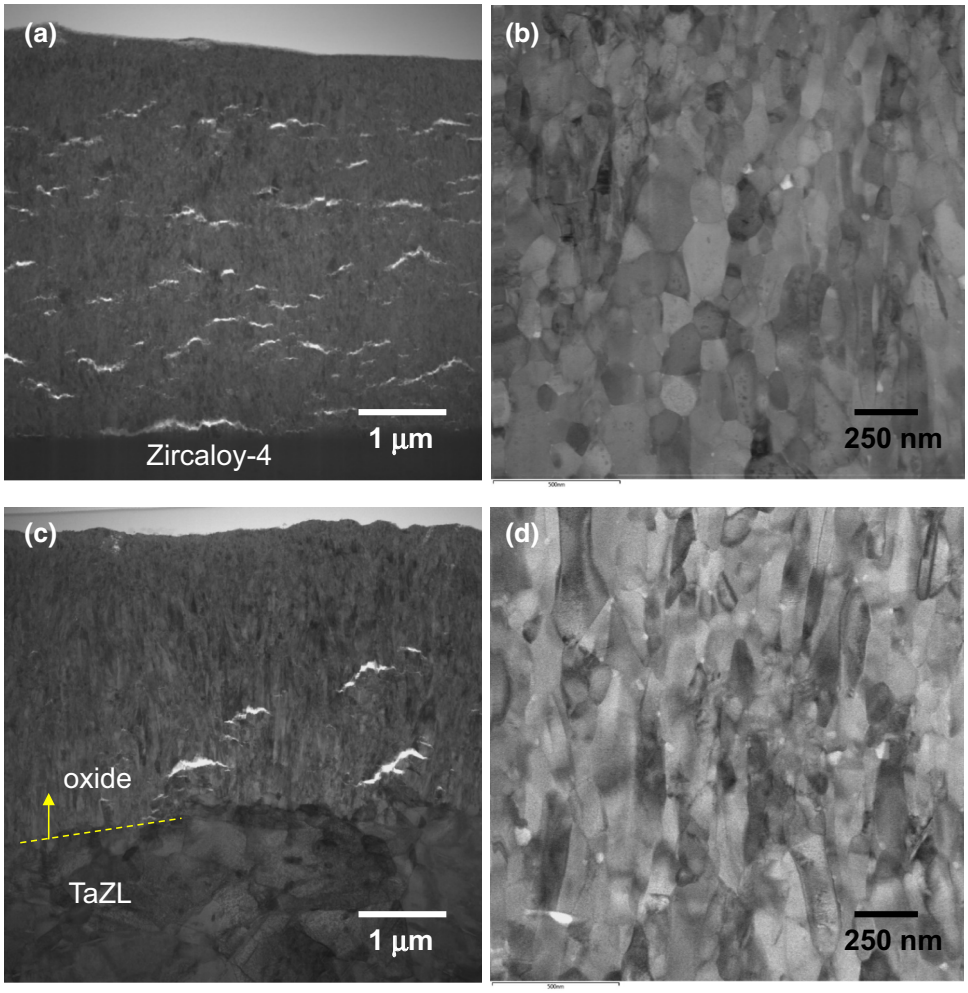


**Fig. 4** Microstructures of the oxides formed on, **a**–**b** Zircaloy-4 and **c**–**d** TaZL samples. **b** and **d** are the magnified versions of **a** and **c**, respectively

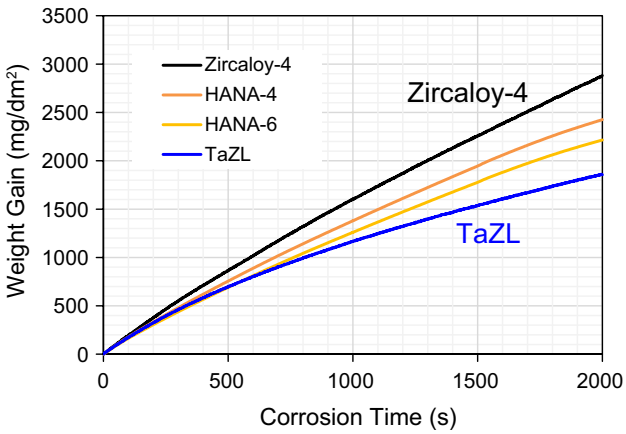


**Fig. 5** **a** Weight gains of TaZL and Zry-4 samples under high-temperature steam oxidation at 1200 °C (included comparable data for HANA alloys [18, 19])

The σ values of Zircaloy-4, ZIRLO, and HANA-4 are 19.73, 19.68, and 20.84, respectively. TaZL has the comparable value of 20.96 as the model alloy was designed to minimize the Ta contents. Thus, TaZL can be used in nuclear fuel cladding materials, and exhibit satisfactory corrosion and oxidation resistance.

## 4 Conclusion

Zr alloy containing 0.03 wt% of Ta as an alloying element was fabricated. The model alloy exhibited low weight gains in the corrosion and oxidation tests. The corrosion of TaZL was 75% less than that of Zircaloy-4. The weight gains were as low as that of the advanced Zr alloy HANA-6. Moreover, no kinetic transition was observed during corrosion up to 840 days. The oxidation in high-temperature steam at 1200 °C was also suppressed by two-thirds compared to that of Zircaloy-4. Ta is expected to stabilize the oxide being formed on Zr surface. Although the evidence of Ta in the oxide layer was not found, the oxides formed on the TaZL samples were thinner and their microstructures were columnar. The positive effect of Ta can be considerable for further development of zirconium alloy.

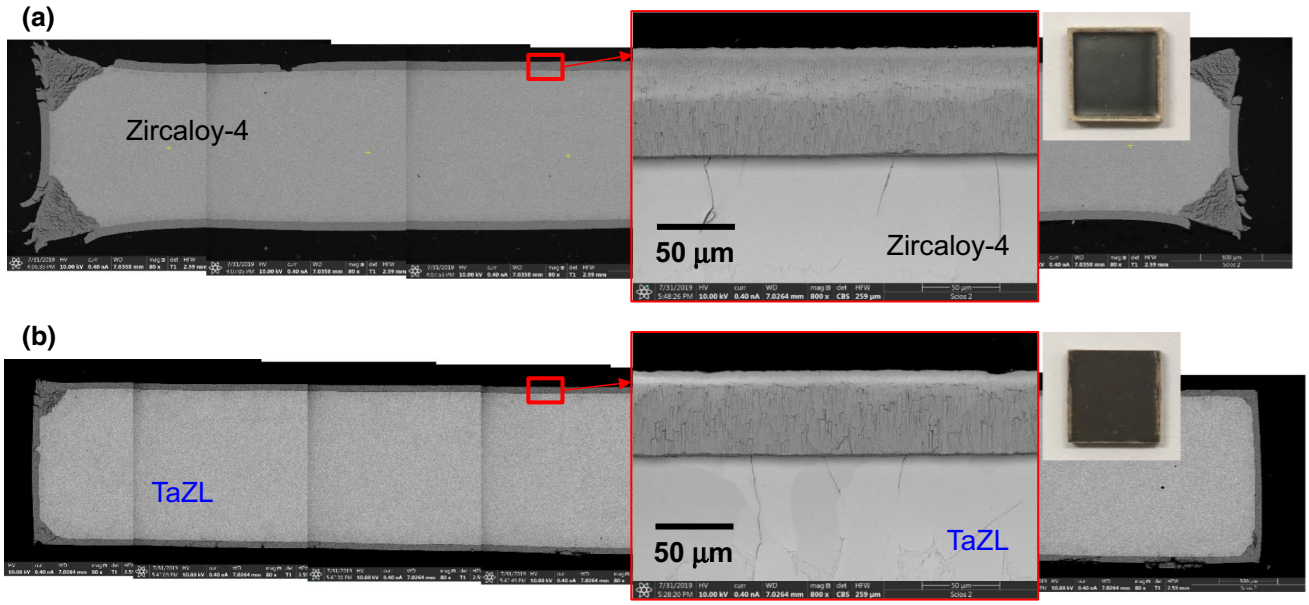


**Fig. 6** Cross-sectional microstructures of samples after high-temperature steam oxidation, showing the oxide layers formed on the surface of, **a** Zircaloy-4 and **b** TaZL

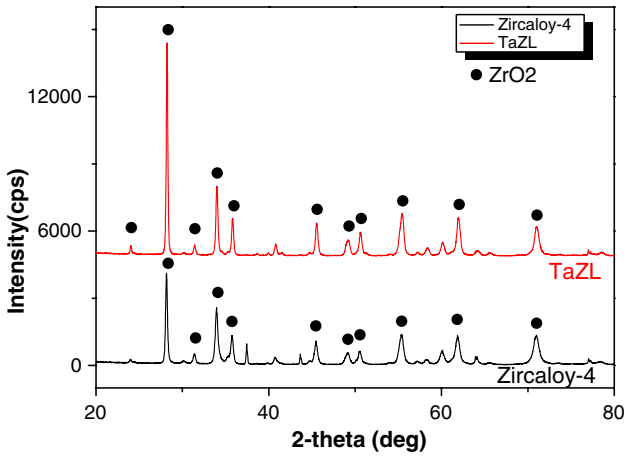


**Fig. 7** X-ray diffraction peaks for oxide layers formed on the Zircaloy-4 and TaZL samples revealing the formation of $ZrO_2$ on both samples

**Acknowledgments** This work was supported by a National Research Foundation of Korea (NRF) grant funded by the Korean government (MSIP) (No. 2017M2A8A5015058).

## References

1. G.R. Sabol, R.J. Comstock, R.A. Weiner, E. Larouere, R.N. Stanutz, In-reactor corrosion performance of ZIRLO™ and Zircaloy-4. Zirconium in the nuclear industry: tenth international symposium, ASTM STP 1245, pp. 724–744 (1994)
2. Y.-H. Jeong, K.O. Lee, H.G. Kim, Correlation between microstructure and corrosion behavior of Zr–Nb binary alloy. J. Nucl. Mater. **302**, 9–19 (2002)
3. H.G. Kim, S.Y. Park, M.H. Lee, Y.H. Jeong, S.D. Kim, Corrosion and microstructural characteristics of Zr–Nb alloys with different Nb contents. J. Nucl. Mater. **373**, 429–432 (2008)
4. K. Takeda, H. Anada, Mechanism of corrosion rate degradation due to tin. Zirconium in the nuclear industry: twelfth international symposium, ASTM STP 1354, pp. 592–608 (2000)
5. P.G. Frankel, J. Wei, E.M. Francis, A. Forsey, N. Ni, et al., Effect of Sn on corrosion mechanisms in advanced Zr-cladding for pressurised water reactors. Zirconium in the nuclear industry: 17th international symposium, ASTM STP 1543, pp. 404–437 (2015)
6. H.-G. Kim, J.-Y. Park, Y.-H. Jeong, Ex-reactor corrosion and oxide characteristics of Zr–Nb–Fe alloys with the Nb/Fe ratio. J. Nucl. Mater. **345**, 1–10 (2005)
7. Y. Broy, F. Garzarolli, A. Seibold, L.E. Van Swam, Influence of transition elements Fe, Cr, and V on long-time corrosion in PWRs. Zirconium in the nuclear industry: twelfth international symposium, ASTM STP 1354, pp. 609–622 (2000)
8. J.-Y. Park, B.-K. Choi, Y.H. Jeong, Y.-H. Jung, Corrosion behavior of Zr alloys with a high Nb content. J. Nucl. Mater. **340**, 237–246 (2005)
9. G.R. Sabol, R.J. Comstock, U.E. Nayak, Effect of dilute alloy additions of molybdenum, niobium, and vanadium on zirconium corrosion. Zirconium in the nuclear industry: twelfth international symposium, ASTM STP 1354, pp. 525–544 (2000)
10. B.D.C. Bell, S.T. Murphy, P.A. Burr et al., The influence of alloying elements on the corrosion of Zr alloys. Corros. Sci. **105**, 36–43 (2016)
11. J. Zhang, Y. Hu, J. Huang, L. Tu, M. Yao, B. Zhou, The corrosion resistance of Zr–0.7Sn–1Nb–0.2Fe–xCu–xGe alloys in 360 °C lithiated water. Corros. Sci. **111**, 132–138 (2016)
12. H. Lee, G.S. Kim, C. Jeon, S.S. Sohn, S.-B. Lee, S.-K. Lee, H.S. Kim, S. Lee, Dynamic tensile deformation behavior of Zr-based amorphous alloy matrix composites reinforced with tungsten or tantalum fibers. Metal. Mater. Int. **22**, 707–713 (2016)

13. H.H. Lee, K.J. Hwang, J. Jung, G.L. Kim, Y.H. Song, S.T. Park, K.W. Oh, H.S. Kim, Grain size effect on mechanical properties under biaxial stretching in pure tantalum. Metal. Mater. Int. **25**, 1448–1456 (2019)
14. J.-Y. Park, S.J. Yoo, B.-K. Choi, Y.H. Jeong, Oxide microstructures of advanced Zr alloys corroded in 360 °C water loop. J. Alloy. Compd. **437**, 274–279 (2007)
15. J.-Y. Park, S.J. Yoo, B.-K. Choi, Y.H. Jeong, Corrosion and oxide characteristics of Zr–1.5Nb–0.4Sn–0.2Fe–0.1Cr alloys in 360 °C pure water and LiOH solution. J. Nucl. Mater. **337**, 343–350 (2008)
16. F. Garzarolli, H. Seidel, R. Tricot, J.P. Gros, Oxide growth mechanism on zirconium alloys. Zirconium in the nuclear industry: ninth international symposium, ASTM STP 1132, pp. 395–415 (1991)
17. H. Anada, T. Takeda, Microstructure of oxides on Zircaloy-4, 1.0Nb Zircaloy-4, and Zircaloy-2 formed in 10.3 MPa steam at 673 K. Zirconium in the nuclear industry: eleventh international symposium, ASTM STP 1295, pp. 35–54 (1996)
18. J.H. Baek, Y.H. Jeong, Steam oxidation of Zr–1.5Nb–0.4Sn–0.2Fe–0.1Cr and Zircaloy-4 at 900–1200 °C. J. Nucl. Mater. **361**, 30–40 (2007)
19. H.-G. Kim, I.-H. Kim, B.-K. Choi, J.-Y. Park, A study of the breakaway oxidation behavior of zirconium cladding materials. J. Nucl. Mater. **418**, 186–197 (2011)